Volume 17
Number 34
14 September 2025
Pages 19479-19968

Nanoscale

rsc.li/nanoscale

ISSN 2040-3372

ROYAL SOCIETY OF CHEMISTRY

PAPER
Simon Maher *et al.*
SERS-based lateral flow immunoassay utilising plasmonic nanoparticle clusters for ultra-sensitive detection of salivary cortisol

NCNST

Nanoscale

PAPER

View Article Online
View Journal | View Issue

Cite this: *Nanoscale*, 2025, **17**, 19656

SERS-based lateral flow immunoassay utilising plasmonic nanoparticle clusters for ultra-sensitive detection of salivary cortisol†

Hyun-Kyung Oh,‡[a] Baris Akbali, ‡[a,b] Tung-Ting Sham, [a] Adam Haworth-Duff,[a] Joanne C. Blair,[c] Barry L. Smith,[a] Nontawat Sricharoen,[d] Cassio Lima, [e] Tsan-Yao Chen,[b] Chen-Han Huang,[f] Kanet Wongravee,[d] Min-Gon Kim, [g] Royston Goodacre [e] and Simon Maher *[a]

Cortisol plays a central role in maintaining physiological homeostasis, and both cortisol excess and deficiency are associated with life-threatening conditions. Accurate diagnosis, adequate treatment and monitoring of disorders of cortisol secretion are essential for good health, normal growth and development. Although commercially available lateral flow immunoassay (LFI) strips can be used to measure cortisol, they have limitations, especially low sensitivity and limited quantitative performance, inhibiting their use in clinical settings. Here, we present a novel LFI platform integrated with surface-enhanced Raman scattering (SERS), employing precisely size-controlled gold nanoparticle clusters functionalised with Raman reporter molecules to overcome these limitations. The approach achieves exceptional sensitivity, covering the relevant therapeutic range in humans, with a limit of detection (LOD) for cortisol of 0.014 pg mL^{-1}, which is >500 times more sensitive than conventional LFI strips. The platform also showed high specificity for cortisol. The diagnostic potential was confirmed by testing with human saliva samples (n = 28), cross-validated with UPLC-MS/MS, showing excellent correlation (R^2 = 0.9977). Bland-Altman analysis demonstrated strong agreement, with all samples falling within the 95% limits and yielding a mean bias of −3.5% ± 13.2% relative to UPLC-MS/MS. Given its sensitivity, specificity and simplicity, this LFI-SERS platform offers strong potential for clinical translation to enable convenient cortisol monitoring.

Received 16th May 2025,
Accepted 22nd July 2025

DOI: 10.1039/d5nr02062j

rsc.li/nanoscale

Introduction

Cortisol is a hormone secreted by the adrenal glands that has a critical role in homeostasis. Symptoms of cortisol deficiency are vague and non-specific and readily attributed to more common conditions.[1] Cortisol secretion increases in response to stress, and children with undiagnosed adrenal insufficiency, who cannot mount a cortisol stress response, may present an 'adrenal crisis', a potentially fatal condition.[2] Symptoms of cortisol excess include slow growth in children,[3] weight gain,[4] hypertension,[5] low mood,[6] metabolic derangement,[7] impaired bone health[8] and symptoms of androgen excess[9] (including acne, facial hair growth in females,[10] male pattern balding[11]). The diagnosis of cortisol deficiency and cortisol excess can be challenging and frequently requires multiple diagnostic tests.

Cortisol secretion shows a circadian profile. Concentrations start to rise in the early hours of the morning, peak 30 min after waking, and then fall throughout the day to very low concentrations overnight.[12] These characteristics of cortisol secretion pose challenges to physicians. Thus, single blood tests are unlikely to be informative unless collected near the time of waking, when cortisol concentrations are high, or at midnight, when cortisol concentrations are low. Samples taken during the day can be useful for assessing cortisol levels during a stress event.[13]

[a]*Department of Electrical Engineering and Electronics, University of Liverpool, UK. E-mail: S.Maher@liverpool.ac.uk*
[b]*Department of Engineering and System Science, National Tsing Hua University, Taiwan*
[c]*Department of Endocrinology, Alder Hey Children's Hospital NHS Foundation Trust, Liverpool, UK*
[d]*Sensor Research Unit, Department of Chemistry, Faculty of Science, Chulalongkorn University, Thailand*
[e]*Centre for Metabolomics Research, Department of Biochemistry, Cell and Systems Biology, Institute of Systems, Molecular and Integrative Biology, University of Liverpool, UK*
[f]*Department of Biomedical Sciences and Engineering, National Central University, Taoyuan 320317, Taiwan*
[g]*Department of Chemistry, Gwangju Institute of Science and Technology, Republic of Korea*

†Electronic supplementary information (ESI) available. See DOI: https://doi.org/10.1039/d5nr02062j

‡These authors contributed equally to this work.

Measurements of cortisol in saliva correlate strongly with measurements in blood samples,[14] and have a number of advantages: sample collection is non-invasive and can be undertaken at home and timed accurately against waking or late at night, multiple samples can be collected during the day, and the cortisol rise in response to venepuncture is avoided. Furthermore, only free, biologically active hormone is measured in contrast to blood tests in which inactive, protein-bound cortisol is also measured,[15] making measurements in saliva more meaningful in states of altered protein binding. Non-invasive tests using saliva are particularly attractive for children.[16,17] Current laboratory techniques for salivary cortisol quantification are complex, time-consuming, require specialist technician expertise, are performed in only a small number of laboratories and are thus impractical for routine clinical practice. Therefore, developing a device that allows regular monitoring by non-experts and facilitates convenient measurement of cortisol would mark a significant breakthrough in clinical management.

Several methods have been explored for hormone detection.[18] Lateral flow immunoassay (LFI) devices have emerged as a popular platform for rapid and convenient point-of-care (POC) diagnostics, offering advantages such as being low-cost, fast, and easy to use – ideal for at-home sampling.[19–22] However, compared to established gold standard measurement methods such as liquid chromatography-mass spectrometry or gas chromatography-mass spectrometry,[23] LFIs exhibit limitations in terms of sensitivity and/or specificity. Therefore, they find their primary utility in qualitative assessments for detecting salivary cortisol concentration within a limited range (typically, ~0.01 to ~10 ng mL^{-1}), which is unsuitable for broader clinical applications.[24] To address this challenge, a more sensitive platform for cortisol monitoring is essential. In response to these limitations, researchers have been actively exploring new platforms that interface LFIs with high-sensitivity analysis methods.[25,26] Among these, surface-enhanced Raman scattering[27] is a promising technique that can be coupled with an LFI test strip. Raman reporter-labelled gold nanoparticles (AuNPs) can be utilised as effective detection probes.[28,29] This allows for quantitative evaluation of biomarkers where SERS stands out as a powerful method due to its ability to deliver fast results,[30] remarkable sensitivity,[31] and resistance to interferences.[32] Raman reporter (RR) molecules[33] that are attached to the surface of nanoparticles experience a significant increase in their SERS signal when they are exposed to an excitation light source at locations on the surface that are known as "hot spots"[34] due to a combination of electromagnetic and chemical enhancement effects. By utilising this method, the level of detection sensitivity can be boosted by up to 10^{14}, which is significantly higher than that of conventional Raman spectroscopy,[35,36] and as such, the development of SERS for clinical diagnostics is increasing in popularity.[27] AuNPs are commonly used in conventional LFI technology and possess excellent biocompatibility with biomolecules such as proteins,[37] antibodies,[38] and DNA.[39]

Several research groups have explored the use of AuNPs,[40,41] hollow AuNPs,[42] and multibranched gold nanostars[43] to fabricate SERS tags, but these often suffer from either weak SERS enhancement or poor colloidal stability. To address these challenges, core–shell composite nanoparticles such as Au@Ag NPs,[44,45] AuNS@SiO_2 NPs,[46] and Au@SiO_2 NPs[47] have recently been explored, offering improved stability while retaining strong SERS activity; however, their synthesis is often complex and difficult to scale. Here, we propose a simplified strategy for SERS tag preparation by promoting the controlled aggregation of AuNPs *via* surface-functionalised RR molecules. This approach enables the formation of strongly SERS-active clusters while significantly simplifying the synthesis process.

In this study, we introduce a novel LFI-SERS platform that combines a precise size-controlled synthesis method incorporating the RR molecule with a Raman mapping-based approach to maximise analytical performance. A central innovation lies in the straightforward formation of well-defined AuNP aggregates using thiol-functionalised RR molecules, which generate strong SERS signals. The size and aggregation of these conjugates were finely tuned, along with the reporter concentration, to optimise their signal on the LFI membrane. By employing Raman mapping across both test and control lines, the platform achieves signal discrimination and quantification accuracy. The optimised LFI-SERS sensor demonstrated an impressive ~650-fold improvement in sensitivity for cortisol detection compared to conventional LFI strips (Table S1, ESI†), supporting its strong potential for clinical utilisation.

Experimental

Chemical and materials

Gold nanoparticles (EM.GC40) were purchased from BBI Solutions (Crumlin, UK), and an anti-cortisol antibody solution (ab1949) was purchased from Abcam (Cambridge, UK). Bovine serum albumin (30-AB74) and surfactant 10G (S10G, 95R-103) were purchased from Fitzgerald Industries International (Acton, MA, USA). Whatman FF080HP membranes (FF080HP) were purchased from GE Healthcare (Chicago, IL, USA), and absorbent (Grade 222), conjugate (6613), and sample pads (Grade 222) were purchased from Ahlstrom-Munksjö (Helsinki, Finland). Borate buffer (28341) was purchased from Thermo Fisher Scientific (Rockford, MD, USA). Phosphate buffered saline (PBS, 1282-1680) and ammonium formate (99%, AC401152500) were purchased from Fisher Scientific UK Limited (Leicestershire, UK). 4-aminothiophenol (≥97.0%), 4-chlorothiophenol (97%), cortisol solution (100 μg mL^{-1} in methanol, C-106), an anti-mouse IgG antibody produced in goat (M8642), polyvinylpyrrolidone (PVP, 10K) (PVP10-100G), Tween® 20 (P1379), and ethyl acetate (≥99.7%, HPLC grade, 34858-1L) were purchased from Sigma-Aldrich Co. (St Louis, Mo, USA). Cortisol-d_4 (1 mg mL^{-1} in methanol, 98% in acetonitrile, QX116168) was purchased from Qmx Laboratories (Essex, UK). All reagent solutions were dissolved in purified water, which passed through a Direct-Q® 3 UV

water purification system (ZRQSVP3WW) from Merck (Rahway, NJ, USA). Methanol (≥99.8%, HPLC Grade) was obtained from VWR (Leicestershire, UK).

Preparation of antibody-conjugated SERS nanotags

To prepare SERS nanotags, 100 μL of 10 μM 4-aminothiophenol (4-ATP) in water was added to 1 mL AuNP solution, vortexed and reacted for 30 min. Then, 100 μL 0.1 M borate (pH 8.5) buffer and 10 μL of 2 mg mL^{-1} anti-cortisol antibodies were added and reacted to adsorb antibodies onto the surface of AuNPs. After 30 min reaction, 10 μL of 10% BSA was added to block unreacted sites on the surface of AuNPs. The solution was allowed to react for another 15 min and then centrifuged at 3968 rcf for 15 min at 10 °C. The solution was washed with water to eliminate non-specific binding of chemicals and antibodies. The supernatant was discarded, and the pellet was resuspended in 1 mL of 10 mM borate buffer (pH 8.5). The centrifugation and cleaning process was repeated 3 more times. The final pellet was re-suspended in 10 mM borate buffer (pH 8.5) to make up to 100 μL, a 10-fold concentrated antibody-conjugated AuNP solution for further use.

Characterisation of AuNP conjugation

For depicting the morphological characteristics of AuNPs, scanning electron microscopy (SEM) imaging was carried out using a Hitachi S4800 scanning electron microscope (Hitachi, Tokyo, Japan) and ultraviolet–visible (UV–Vis) spectroscopy was carried out with a UV–Vis spectrometer (Genesys 10S UV–Vis spectrophotometer, Thermo Fisher Scientific, Rockford, MD, USA). Dynamic light scattering (DLS) measurements (Zetasizer Nano Particle Sizer, Malvern Panalytical, Malvern, UK) were also carried out to analyse the AuNPs sizes before and after conjugation.

Preparation of LFI sensor strips

To prepare an LFI strip sensor, 0.5 mg mL^{-1} of anti-mouse IgG antibody and 0.25 mg mL^{-1} of cortisol-BSA were immobilised on a nitrocellulose membrane (1.25 μL cm^{-1}) to act as the control line and test line, respectively. A dispenser (Automated Lateral Flow Reagent Dispenser, ClaremontBio, CA, USA) and a cutting device (TBC-50Tx, Taewoo Co., Namyangju, South Korea) were used to immobilise antibodies onto the membrane and then cut the membrane, respectively. The distance between the lines was consistent between LFI sensors and was approximately 4 mm. The membrane was cut with 3 mm width, and an absorbance pad (3 × 20 mm^2) was attached to the top of the membrane with 2 mm overlap. The aggregated gold nanoparticles conjugate solution (6.5 μL, 0.1-fold concentration) with assay buffer (1% polyvinylpyrrolidone-10K, 0.5% surfactant 10G in 10 mM borate (pH 8.5)) were applied to the conjugate pad (3 × 5 mm^2). After drying the conjugate pad at 37 °C for 30 min, it was attached to the bottom of the membrane with 2 mm overlap, and the sample pad (3 × 20 mm^2) was attached to the bottom of the conjugate pad with 4 mm overlap. This strip was stored in a humidity-controlled chamber (21 °C and 23% relative humidity) until use.

Sensitivity and specificity of the LFI sensor strip

A standard of cortisol was first dissolved in methanol and diluted in water with different concentrations for application to the LFI sensor strips. Next, 100 μL of the prepared sample solutions were applied to the LFI sensors and incubated at room temperature for 15 min. To test specificity, other steroid hormones, including cortisone, corticosterone, progesterone, and estrone, were also prepared in methanol first and then diluted in water at concentrations of 10 pg mL^{-1} and 1 ng mL^{-1} for applying to the LFI sensor. After the assay, all images were obtained using a GelDoc Go imaging system (Bio-Rad Laboratories, Inc., CA, USA), and the Raman spectral signal was measured using a Renishaw Raman microscope (details provided below).

SERS mapping of test and control lines on the LFI sensor strip

The test and control line of each strip was analysed using an inVia™ Confocal Raman microscope system (Renishaw, New Mills, UK) to obtain Raman spectra and SERS mapping images. A 3 mW He–Ne laser at λ = 785 nm was used for excitation. The collected Raman data were processed to remove the Rayleigh line using a holographic notch filter. A charge-coupled device (CCD) camera and a spectrograph were used to achieve a combined spectral resolution of 1 cm^{-1}. A computer-controlled x–y translational stage was scanned over a range of 2500 μm (x-axis) and 150 μm (y-axis) in steps of 50 μm × 100 μm. The data acquisition time for each measurement point was set to 2 s, and any cosmic rays were removed from the spectra after each scan using the WiRE™ software V 4.0 (Renishaw, New Mills, UK). The objective lens used in this study has a numerical aperture of 0.75. SERS maps were processed using MATLAB (Mathworks, MA, USA), monitoring the characteristic peak intensity of 4-ATP at 1585 cm^{-1}.

Data processing

The raw Raman spectra were exported from WiRE™ software in text format for further analysis using MATLAB. The exported data included Raman wavenumber intensity values as well as x and y coordinate information. These data were imported into a table data structure in MATLAB and underwent a standardised processing procedure, which involved the following steps:

1. Smoothing of the intensity data using a Savitzky–Golay filter with a window width of 15 bins to reduce noise and improve data quality.

2. Baseline correction was carried out by estimating the baseline within multiple shifted windows of 60 separation units. Spline approximation was then used to perform regression and correct for any baseline variation.

3. Wavenumber-specific intensity information of interest was extracted at each x and y coordinate, allowing the generation of heat maps to visualise the distribution of the analyte across the surface.

For each LFI-SERS sensor measurement, a total of 300 data points were collected (150 from the test line and 150 from the control line). To ensure data accuracy, a data trimming process

was applied, removing outliers from the top and bottom 10% of the dataset. This outlier removal step enhanced the reliability of the analysis. After the outliers were removed, the average SERS intensity was calculated based on the remaining data points.

Cross-validation of LFI-SERS platform with human saliva samples

To evaluate the impact of variation in individual saliva matrices, seven healthy adult volunteers (women, 3; men, 4; average age = 34 ± 7.8) were recruited for the study with requisite ethical approval (University of Liverpool Research Ethics Committee, approval reference number: 14651). Written informed consent was obtained from all participants prior to sample collection in accordance with the Declaration of Helsinki. LFI cross-validation with ultra-performance liquid chromatography-tandem mass spectrometry (UPLC-MS/MS) analysis involved three main steps as outlined below.

I. Human saliva sample collection

Participants were asked to refrain from eating or drinking at least 1 h before sample collection. To stimulate saliva production in these participants, saliva samples were collected by gently chewing with a cotton swab for at least 2 min at 4-time points (each at ≥2 h intervals). The samples were immediately frozen at −20 °C for at least 24 h. They were thawed and centrifuged at 18 407 rcf at 4 °C for 20 min to remove any precipitate or oral debris before being aliquoted for analysis.

II. LFI-SERS analysis

Calibration solutions at 0, 0.05–100 ng mL^{-1} were prepared from 1 μg mL^{-1} of cortisol using water. 100 μL of calibration solutions and 10-fold diluted (with water) saliva samples were applied to the LFI sensor in each case prior to SERS mapping and data processing.

III. UPLC-MS/MS analysis

UPLC-MS/MS analysis is widely considered a gold standard method for cortisol measurement.[48–50] To verify the accuracy of LFI-SERS quantification, a UPLC-MS/MS analysis was performed as a cross-validation method. The UPLC-MS/MS procedure was adapted from two well-established cortisol quantification protocols of Anderson *et al.*[51] and Ray *et al.*[48] Modifications were made where necessary to optimise the sample extraction and UPLC-MS/MS performance for the specific saliva sample matrix and concentration range analysed in this study. The following are the methodological details.

(IIIa) Liquid–liquid extraction of cortisol

150 μL saliva samples were aliquoted to 1.5 mL centrifuge tubes and spiked with 15 μL 100 ng mL^{-1} of cortisol-d_4 internal standard solution (50% methanol in water). They were vortexed for 1 min. 150 μL 100% ethyl acetate was added to the sample, vortexed for 1 min, and centrifuged at 18 407 rcf at 4 °C for 10 min. The upper layer of ethyl acetate extract was transferred to a 1.5 mL centrifuge tube and gently dried under nitrogen gas. The whole extraction procedure was repeated once. The second ethyl acetate extract was added to the same centrifuge tube and dried again. 75 μL of 25% methanol in water with 0.5 mM ammonium formate was added to reconstitute cortisol. The mixture was vortexed for 1 min and centrifuged at 18 407 rcf at 4 °C for 10 min. The supernatant was transferred into a glass insert with an HPLC vial. Calibration solutions at 0, 0.05–100 ng mL^{-1} were processed in the same manner as the saliva samples.

(IIIb) UPLC-MS/MS method

The UPLC-MS/MS analysis was carried out on a Waters ACQUITY UPLC system (Waters Corporation, Milford, MA). The injection volume was 10 μL. UPLC separation was performed on a Waters ACQUITY UPLC BEH Phenyl column (2.1 mm × 100 mm, 1.7 μm) with a BEH Phenyl guard column (2.1 mm × 5 mm, 1.7 μm). The mobile phase consisted of combinations of A (0.5 mM ammonium formate in water) and B (0.5 mM ammonium formate in 95% acetonitrile with 5% water, v/v) at a flow rate of 0.3 mL min^{-1} with an elution gradient as follows: 0–0.5 min, 25% B; 0.51–4.0 min, 35% B; 4.01–6.5 min, 100% B. A 3.5 min post-run time was set to fully equilibrate the column. Column and sample chamber temperatures were 40 °C and 6 °C, respectively. Mass spectrometry analysis was conducted with a Waters Xevo triple quadrupole mass spectrometer (Waters, Milford, USA) with electrospray ionisation in positive mode. Desolvation and cone gases used nitrogen set at 800 L h^{-1} and 150 L h^{-1}, respectively. The desolvation and source temperatures were kept at 500 °C and 150 °C, respectively. The source capillary voltage was 3.5 kV. Argon was used as the collision gas. The multiple reaction monitoring (MRM) transitions were: m/z 363.22 → 121.05 as a quantifier, m/z 363.22 → 91.02 as a qualifier for cortisol, and m/z 367.24 → 121.06 as a quantifier for cortisol-d_4. The optimised parameters for the three MRM transitions were: cone voltage, 38 V, 38 V and 40 V, respectively; collision energy: 26, 60 and 24 eV, respectively. The dwell time was 0.063 s per transition. Peaks were integrated using TargetLynx V4.1 SCN 901 (Waters, Milford, USA), and the peak area ratio of the quantifiers of cortisol to that of cortisol-d_4 were used for quantification.

Results and discussion

Scheme of LFI-SERS sensor

The LFI-SERS sensing platform is based on a LFI strip composed of a sample pad, conjugate pad, nitrocellulose membrane (containing a test and control line), and an absorbent pad (Fig. 1a). The strip is specifically designed to detect cortisol in human saliva samples. Once the sample is applied to the sample pad, it flows through the strip *via* capillary action to initiate the detection process. A key innovation of this study lies in our controlled aggregation strategy for gold nanoparticles, achieved by finely tuning the concentration of RR molecules. This tuning adjusts the localised surface plasmon resonance, enhancing the optical and SERS properties of the nanoparticle conjugates. Furthermore, the use of Raman mapping at both the test and control lines enables us to average the SERS signal intensities, thereby minimising the impact of local signal fluctuations caused by nanoparticle aggregation or distribution inhomogeneity. This results in a

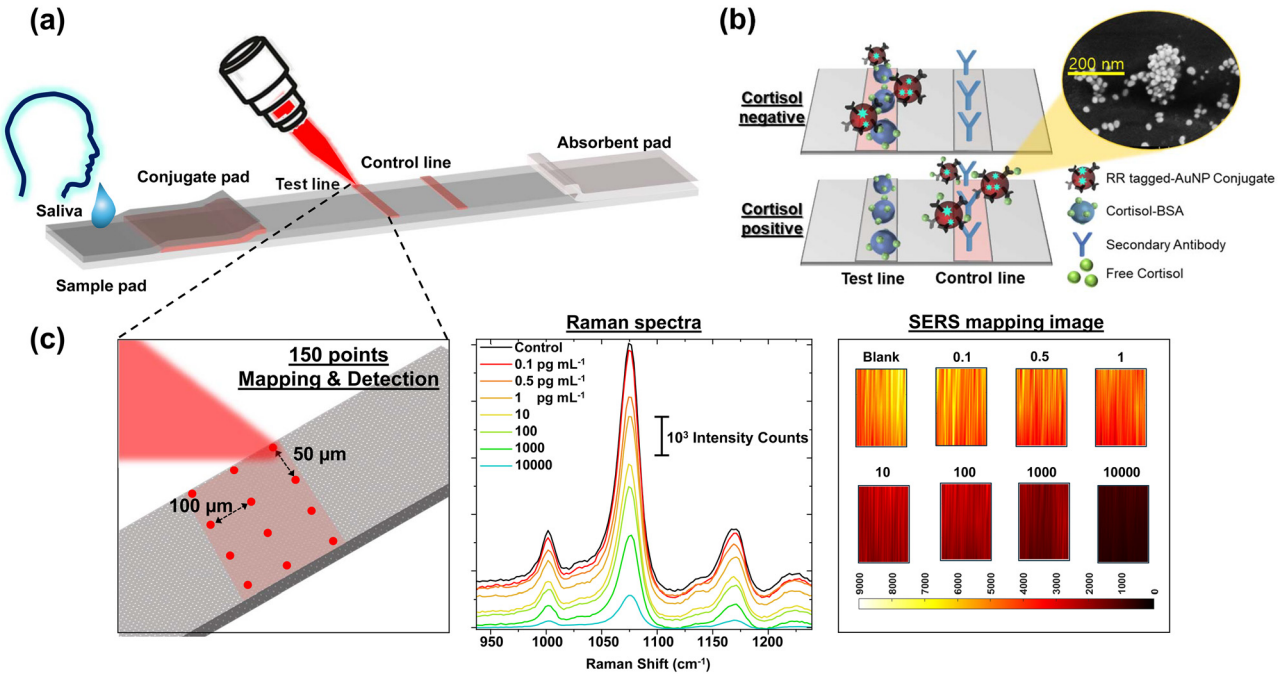

Fig. 1 Schematic illustration of the LFI-SERS sensing platform. (a) The LFI-SERS sensor strip comprises a sample pad, conjugate pad, test line, control line, and absorbent pad. After immunoassay, a Raman signal is obtained using a Raman microscope system. (b) In the absence of the target antigen (negative), optimised concentration of conjugate binds to the test line, while in the presence of the target antigen (positive) it binds to the control line. (c) Raman mapping is performed across test and control lines (left), yielding Raman spectra (middle), which are also displayed as a series of intensity colour maps (right).

more robust, reliable, and reproducible quantification method on the LFI sensor strip. Notably, the control line retains its conventional role in confirming strip functionality while also serving as an internal reference for ratiometric quantification.

The sample migrates through the conjugate pad, where aggregated gold nanoparticles (AuNPs) are conjugated with cortisol antibodies and RR molecules, namely 4-ATP. The RR-tagged AuNP conjugates serve as the detection probe for cortisol, as depicted in Fig. 1b. At the test line, the nitrocellulose membrane is coated with cortisol-protein conjugate to capture cortisol antibodies, and anti-mouse secondary antibodies are immobilised on the control line. The test line competes with cortisol molecules for conjugate binding, and the control line offers dual utility. In addition to verifying the overall functionality of the assay, the control line further serves as a unique second test line for cortisol detection. As shown in Fig. 1c, a distinct feature of the approach used in this study to aid quantitation lies in the diametric signalling outcomes of the test and control lines, which require an optimal amount of conjugate to operate effectively. While the test line exhibits a signal in the absence of cortisol, in contrast, the control line shows a signal in the presence of cortisol (Fig. 1b). The small molecule cortisol can be accurately quantified by leveraging these opposing signal intensities. After the immunoreaction, a laser excites the RR molecules attached to the aggregated AuNPs. The laser light interacts with the RR molecules, causing them to emit a characteristic Raman scattering signal. A mapping system is employed to scan a significant portion of the test and control strip areas on the LFI, allowing the average Raman signal intensity associated with a characteristic wavenumber to be calculated. The intensity ratio between the test and control lines serves as the basis for quantifying the cortisol concentration in the sample (Fig. 1c), normalising strip-to-strip variation and flow heterogeneity.[52]

Characterisation of aggregated gold nanoparticles

To prepare an aggregated SERS nanotag, 4-ATP was attached to an AuNP. The 4-ATP molecule was chosen as a RR molecule due to its high binding efficiency on gold surfaces. Different concentrations of 4-ATP (10 μg mL^{-1} and 50 μg mL^{-1} dissolved in water) were introduced into the colloidal AuNP solution and reacted for 20 min by stirring. To act as a control, 4-chlorothiophenol (4-CTP), which belongs to the same family of RR molecules but lacks binding affinity for a metal surface, was used. The visual appearance of the colloidal solutions changed under daylight conditions due to alterations in their plasmon activity, as shown in Fig. 2a. In comparison to the bare colloidal AuNP solution (Fig. 2a left), the colour of the solutions exposed to 4-ATP molecules became progressively darker, with the intensity of the colour change correlating to the concentration of 4-ATP (10 μg mL^{-1} for Fig. 2a middle and 50 μg mL^{-1} for Fig. 2a right). UV-Vis was used to investigate the changes in the plasmonic band upon addition of the RR, as depicted in Fig. 2b. The spectrum revealed a distinct peak at

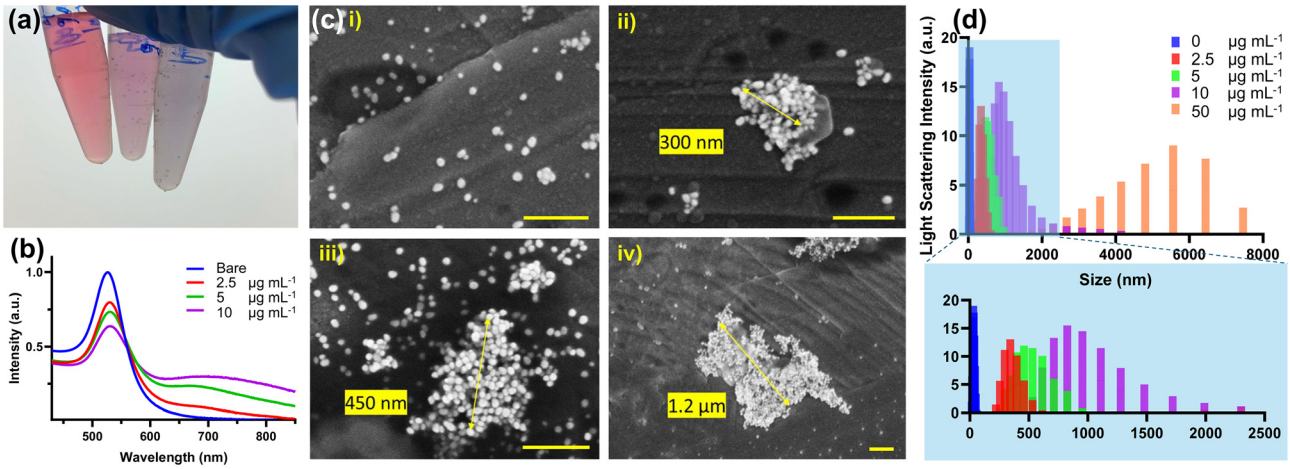

Fig. 2 Characterisation of gold nanoparticle clusters (a) photograph of colloidal AuNP solutions (left: bare AuNP colloidal solution; middle: AuNP solution with μg mL^{-1} 4-ATP; right: AuNP solution with 50 μg mL^{-1} 4-ATP), (b) UV–VIS absorption spectra, (c) scanning electron micros-copy (SEM) images of AuNPs with (i) 0 μg mL^{-1} (bare), (ii) 2.5 μg mL^{-1}, (iii) 5 μg mL^{-1}, and (iv) 10 μg mL^{-1} 4-ATP addition, and (d) dynamic light scattering (DLS) size measurements. All scale bars are 250 nm.

525 nm, indicating a uniform size distribution of the nanoparticles. However, upon addition of varying amounts of 4-ATP to the AuNP solution, a second surface plasmon resonance (SPR) band emerged around 690 nm. Notably, as the nanoparticle size increased due to aggregation, a red shift in the second SPR band was observed, indicating enhanced aggregation and larger cluster formation. The increased aggregation resulted in a higher number of 4-ATP molecules being tagged to the gold nanoparticles, leading to stronger SERS signals and improved particle sensitivity.

The synthesised conjugate was confirmed by Raman spectroscopy, which exhibited a signal difference of approximately 1000 times (or more) compared to the control conjugate using 4-CTP (Fig. S1a†). Additionally, in the case of the control conjugate, no aggregation was observed in the SEM images (Fig. S1b†), and there was no colour change in the absorbance spectrum (Fig. S1c†). SEM images of the AuNPs are presented in Fig. 2c, revealing their aggregation behaviour. It is evident from the images that in the absence of the RR molecule, the AuNPs do not exhibit significant aggregation. However, as the concentration of 4-ATP increases, the size of the nanoparticle aggregates progressively grows, indicating a direct correlation between the concentration of 4-ATP and the extent of nanoparticle aggregation. The size of the aggregated AuNPs was further characterised using dynamic light scattering (DLS) measurements, as shown in Fig. 2d. The results indicate that the degree of aggregation is dependent on the amount of RR molecule added. When a smaller amount of RR is used, the nanoparticle aggregation is relatively minor, whereas a larger amount of RR molecules leads to increased nanoparticle aggregation. This is supported by the median values obtained from the DLS measurements, which were 28.2, 342, 459, 825, and 5560 nm for 0, 2.5, 5, 10, and 50 μg mL^{-1} concentrations of RR molecule, respectively. This result is consistent with the observations from the SEM images presented in Fig. 2c, providing additional support for the findings.

Reproducibility testing demonstrated consistent results across three measurements. Four different concentrations, 2.5, 5, 10, and 50 μg mL^{-1}, were tested to find the optimum concentration of RR molecule to be added. 10 μg mL^{-1} and 50 μg mL^{-1} additions of RR molecule display large and non-uniform aggregation. Aggregation larger than 500 nm should be avoided as the particle sizes become larger than the size of the nitrocellulose pores. The addition of 2.5 μg mL^{-1} and 5 μg mL^{-1} 4-ATP shows good aggregation size uniformity, but 5 μg mL^{-1} gives a slightly increased SERS signal than 2.5 μg mL^{-1} (Fig. S2†). Therefore, 5 μg mL^{-1} was chosen as the optimal amount of RR to be introduced into the aggregated AuNP solution. This concentration was determined as optimal not only based on the balance between signal intensity and aggregation uniformity, but also considering the compatibility with the LFI membrane pore size and the stability of the signal across repeated measurements. Ensuring that the nanoparticle aggregates remain below the membrane pore size is critical for consistent flow, efficient immobilisation at the test and control lines, and robust signal reproducibility in the LFI-SERS platform.

Stability tests showed that the aggregated AuNPs were sufficiently stable, retaining their aggregated form for at least one week (Fig. S3†). Finally, the synthesised conjugate was applied to an LFI strip to validate the Raman signal. The aggregated AuNP conjugate utilising 4-ATP exhibited a significantly high average signal, exceeding 30 000, whereas the control AuNP conjugate, employing 4-CTP as the RR, displayed a much lower average signal of approximately 1000 (Fig. 3).

Detection of cortisol using aggregated gold nanoparticle conjugates

The standard solution, containing 1% poly-vinylpyrrolidone (10 000 Da) and 0.5% surfactant 10G in 10 mM borate buffer

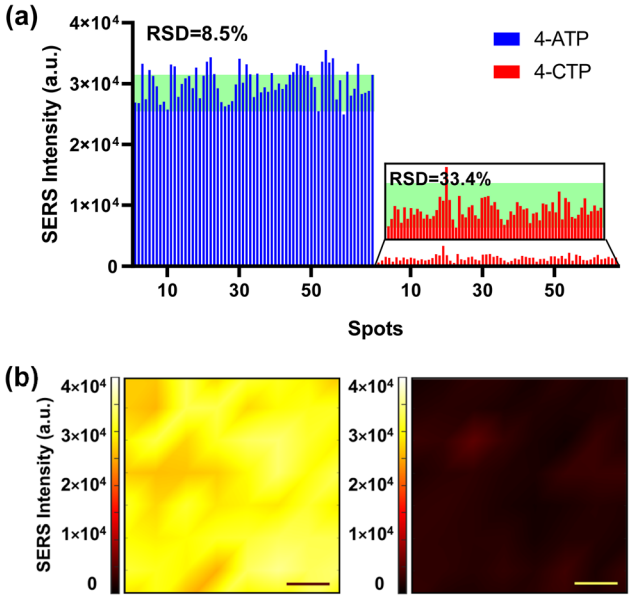

Fig. 3 Raman (SERS) intensity of AuNP conjugate with 4-aminothiophenol (4-ATP) or 4-chlorothiophenol (4-CTP) from the test line of a LFI strip. (a) Raman intensity of different mapping spots (for 4-ATP, the mean is 30 202.39 with a relative standard deviation (RSD) of 8.5%, and for 4-CTP, the mean is 1361.12 with an RSD of 33.4%), (b) colour map showing signal intensity across the area measured on the LFI strip. SERS mapping measurements were conducted on a 25 × 25 μm^2 area with a step size of 3 × 3 μm. The scale bar in the images represents 5 μm.

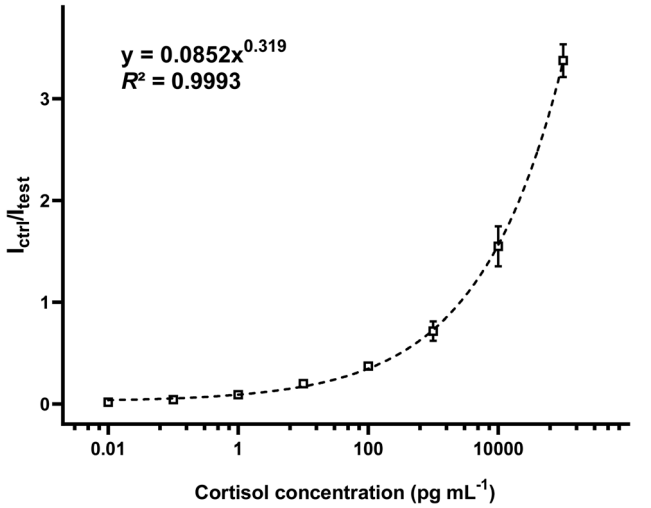

Fig. 4 Sensitivity of LFI-SERS sensor for cortisol detection. The graph shows the sensor's response to cortisol concentrations ranging from 0.01 pg mL^{-1} to 100 ng mL^{-1}. The square open symbols with error bars represent the means ± SD (n = 3).

(pH 8.5), was applied to the sample pad of the strip prepared as described in the Experimental section. The Raman scattering intensity was measured using a confocal Raman microscope and WiRE™ software. The results were analysed using MATLAB software to quantify the signal intensities on the strips.

SERS is a highly sensitive technique, but reliably measuring a Raman signal from a test or control line can be challenging due to the inherent non-uniform distribution of conjugated gold nanoparticles (AuNPs) across the LFI strip. This variation can result from uneven flow, aggregation behaviour, or differences in local substrate morphology, all of which can affect signal reproducibility. To mitigate these effects, Raman mapping was employed across both test and control lines, collecting approximately 300 spectra per LFI sensor.

To account for signal deviation caused by local aggregation or surface inhomogeneities, we calculated the average SERS intensity separately for the test and control lines. By averaging these mapped intensities, we minimised the influence of localised "hot spots" or weak signal zones. The processed average Raman scattering intensities were then used to construct a calibration plot of Raman intensity *versus* cortisol concentration, fitted using a sigmoidal function for concentrations ranging from 0.01 pg mL^{-1} to 100 ng mL^{-1} (Fig. 4). The limit of detection (LOD) for the LFI-SERS sensing platform was calculated to be 0.014 pg mL^{-1} based on the sum of the mean blank signal and three times its standard deviation.[53] This LOD is approximately 650 times lower than previously reported values using conventional antibody-conjugated AuNPs.[26] A comparison with previously published literature (Table S1, ESI†) further highlights the sensitivity of our approach.

Specificity test using other steroid hormones

To assess the selectivity of the LFI-SERS sensor, a comprehensive series of experiments was conducted to detect various steroid hormones, including cortisol, cortisone, corticosterone (CORT), progesterone (P4), and estrone (E), at concentrations of 10 pg mL^{-1} and 1 ng mL^{-1}. The experimental procedures and characterisation methods employed were consistent with those described earlier, utilising a confocal Raman microscope and MATLAB software to acquire and analyse Raman scattering signals. The specificity tests yielded important insights into the selectivity of the LFI-SERS sensor regarding its capability to detect cortisol from other steroid hormones. Fig. 5a and b visually represent the outcomes of the specificity test, showcasing the distinct response of the LFI-SERS sensor to the different steroid hormones tested. The results demonstrated the high selectivity towards cortisol, as evidenced by the significant differences in the Raman scattering signals when cortisol was tested compared to other steroid hormones at both concentrations (10 pg mL^{-1} and 1 ng mL^{-1}).

Clinical validation with saliva samples using UPLC-MS/MS

To evaluate the real-world performance, we conducted an initial validation study using 28 human saliva samples. Each sample was also analysed using UPLC-MS/MS, serving as a reference method. Cortisol concentrations measured by the LFI-SERS platform were compared with those from UPLC-MS/MS (Fig. 6), revealing excellent agreement. The coefficient of determination (R^2 = 0.9977) indicated a strong linear corre-

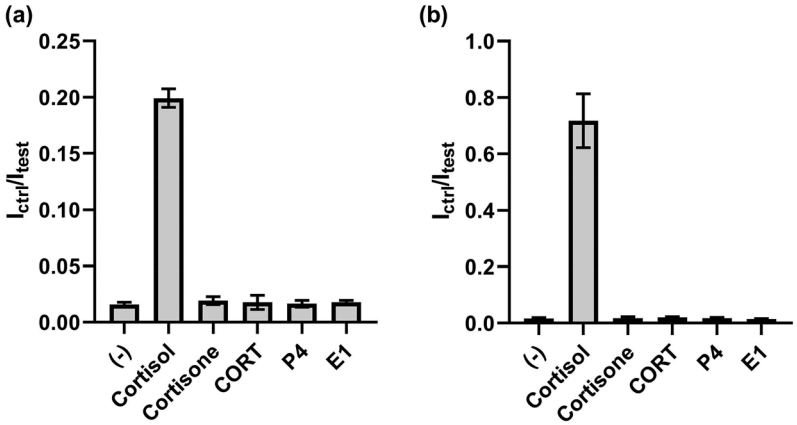

Fig. 5 Selectivity assay for steroid hormones, showing the response of the sensor to solutions containing (a) 10 pg mL^{-1} and (b) 1 ng mL^{-1} of cortisol, cortisone, corticosterone (CORT), progesterone (P4), and estrone (E). Bars show signal means ± SD (n = 3).

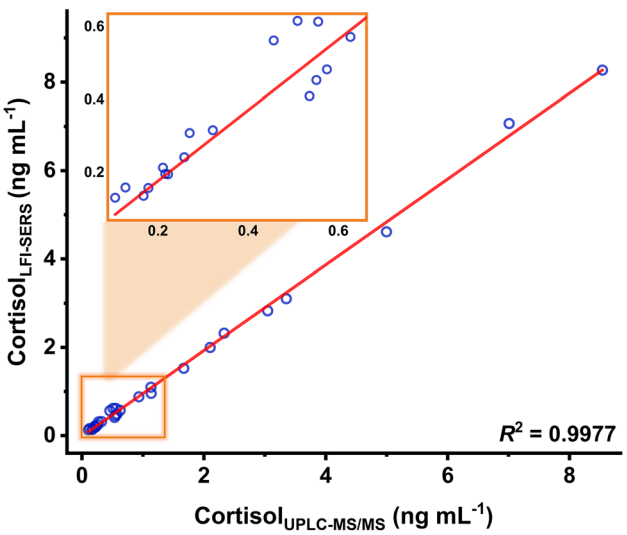

Fig. 6 Correlation between human salivary cortisol levels measured by UPLC-MS/MS and those by LFI-SERS. The inset provides a zoomed-in view of the same plot, focusing on a narrower concentration range close to the origin.

lation between the two techniques. Agreement was further assessed using Bland-Altman analysis (Fig. S4†), where all samples fell within the 95% limits of agreement, with a mean bias of −3.5% ± 13.2% relative to UPLC-MS/MS. Representative UPLC-MS/MS chromatograms and the calibration curve are shown in Fig. S5 and S6,† respectively. These results demonstrate the clinical viability of the LFI-SERS platform for salivary cortisol analysis.

Clinical prospects

This study marks a substantial achievement in cortisol detection by integrating SERS with LFI, achieving a detection limit of 0.014 pg mL^{-1} – over 650 times more sensitive than conventional LFI methods. Previous LFI studies have reported detection limits around 9.1 pg mL^{-1}.[26] Although other SERS-based LFI platforms have shown improved sensitivity, they are not suited for small-molecule analysis.[54,55]

A key innovation of this platform is the use of controlled AuNP aggregation to amplify SERS signals from the Raman reporter, yielding significantly improved sensitivity compared to studies using non-aggregated NPs.[28,49,55] Additionally, instead of relying solely on the test line for quantification, cortisol levels were determined based on the intensity ratio of the control line over the test line. This strategy enhances accuracy and reduces variability. Moreover, initial stability tests indicated that the aggregated AuNPs maintain their form for at least one week (Fig. S3†), which is very promising at this stage. Comprehensive testing (over extended durations at a range of temperatures and humidities) is beyond the scope of this initial proof-of-concept study and remains the focus of future work as we seek to translate this platform for clinical use.

The strong correlation with UPLC-MS/MS (R^2 = 0.9977 across 28 saliva samples) underscores the clinical relevance and accuracy of this approach. Importantly, saliva as a sampling matrix offers distinct advantages for real-world applications, particularly in paediatric and outpatient settings, due to its non-invasive, painless collection and reduced physiological disruption, including avoidance of venepuncture-induced cortisol spikes. This enhances the feasibility of frequent, at-home monitoring for chronic conditions involving cortisol dysregulation. The LFI-SERS sensor is well-suited for deployment across diverse use cases, including early diagnosis, decentralised testing, and PoC monitoring *via* portable Raman readers. Such systems could streamline cortisol assessment and support more responsive, personalised clinical management.

Conclusions

This study presents an LFI-SERS sensing platform for the highly sensitive and accurate detection of cortisol from human saliva samples. Limitations of conventional LFI methods are addressed by incorporating aggregated AuNP conjugates with a

Raman reporter molecule, 4-ATP, acting as the detection probe. The optimised synthesis method allowed precise control of the size and aggregation of the AuNPs, resulting in enhanced sensitivity for cortisol detection. The synthesised conjugate demonstrated a significantly higher Raman signal compared to the control conjugate, indicating the successful attachment of 4-ATP to the AuNPs and the formation of stable aggregates. The visual appearance and UV–Vis spectra of the solutions confirmed the concentration-dependent plasmon activity and aggregation of the AuNPs. Furthermore, the size and aggregation behaviour of the AuNPs were further characterised using SEM and DLS measurements, which revealed a direct correlation between the concentration of 4-ATP and the extent of nanoparticle aggregation.

The optimised LFI-SERS sensing platform exhibited exceptional sensitivity, with a LOD of 0.014 pg mL^{-1} for cortisol. High selectivity towards cortisol was also observed, as demonstrated by the negligible interference from other steroid hormones. Furthermore, pre-clinical validation using human saliva samples (n = 28) showed excellent correlation between the cortisol concentrations measured by the LFI-SERS platform and UPLC-MS/MS (R^2 = 0.9977), indicating its suitability for further clinical application. As SERS has already been successfully miniaturised into a handheld/portable format,[49] there is potential to employ this approach in a PoC setting in future work. Validation studies in larger cohorts are warranted to fully explore the potential of this platform in a clinical setting.

Author contributions

H. K. O. and B. A. undertook key experiments and day-to-day developments under the supervision of S. M., as well as contributing to writing the original draft and subsequent revisions. B. A., H. K. O., T. T. S., and A. H. D. performed the synthesis and characterisation of the AuNP-conjugated LFI strips. B. A. carried out the SERS mapping and SEM imaging experiments. T. T. S. conducted the UPLC-MS/MS analysis and prepared the results in a publishable format. N. S. and C. L. contributed to the initial experimental design and provided valuable feedback on the manuscript. B. L. S., T. Y. C., C. H. H., K. W., M. G. K. and R. G., offered valuable insights, feedback and critical revisions to the study and the corresponding manuscript. S. M. conceptualised and led the study with support from B. A., H. K. O. and J. C. B.

Conflicts of interest

There are no conflicts to declare.

Data availability

The data supporting the findings of this study involve human saliva samples and are subject to ethical and confidentiality restrictions. As such, they are not publicly available. All relevant data are presented within the article and its ESI.†

Acknowledgements

B. A. acknowledges funding from the University of Liverpool and National Tsing Hua University (NTHU) partnership. S. M. and R. G. are extremely grateful for the support received from the EPSRC (EP/V001019/1). J. B. and S. M. are grateful for support from The Gabriel Trust, the charitable foundation of David and Maureen Speakman. S. M., K. W. and N. S. acknowledge support from the National Science, Research and Innovation Fund (NSRF) *via* the Program Management Unit for Human Resources & Institutional Development, Research and Innovation (B16F640101). T. T. S extends her gratitude to Dr Steven Robinson and Dr Megan Carr for their technical support with UPLC-MS/MS and B. A. extends appreciation to Mr. Owen Gallagher for his assistance with SEM imaging at the Materials Innovation Factory, University of Liverpool.

References

1 B. Bleicken, M. Ventz, M. Quinkler and S. Hahner, *Am. J. Med. Sci.*, 2010, **339**, 525–531.
2 C. E. Martinelli, S. L. Sader, E. B. Oliveira, J. C. Daneluzzi and A. C. Moreira, *Clin. Endocrinol.*, 1999, **51**, 67–71.
3 S. A. Bowden, *Pediatr. Health, Med. Ther.*, 2023, 117–130.
4 S. D. Hewagalamulage, T. Lee, I. Clarke and B. Henry, *Domest. Anim. Endocrinol.*, 2016, **56**, S112–S120.
5 J. J. Kelly, G. Mangos, P. M. Williamson and J. A. Whitworth, *Clin. Exp. Pharmacol. Physiol.*, 1998, **25**, S51–S56.
6 O. M. Wolkowitz, H. Burke, E. S. Epel and V. I. Reus, *Ann. N. Y. Acad. Sci.*, 2009, **1179**, 19–40.
7 P. Anagnostis, V. G. Athyros, K. Tziomalos, A. Karagiannis and D. P. Mikhailidis, *J. Clin. Endocrinol. Metab.*, 2009, **94**, 2692–2701.
8 B.-J. Kim, M. Kwak, S. Ahn, J. Kim, S. Lee and J.-M. Koh, *Osteoporosis Int.*, 2018, **29**, 2299–2307.
9 L. Laue, G. L. Peck, D. L. Loriaux, W. Gallucci and G. P. Chrousos, *J. Clin. Endocrinol. Metab.*, 1991, **73**, 380–384.
10 J. G. Nejad, M. Ghaseminezhad, K. Sung, F. Hoseinzadeh, J. Cabibi and J. Lee, *J. Steroids Horm. Sci.*, 2016, **7**, 177.
11 M. I. New, *Ann. N. Y. Acad. Sci.*, 2004, **1038**, 14–43.
12 N. A. O'Byrne, F. Yuen, W. Z. Butt and P. Y. Liu, *Curr. Opin. Endocr. Metab. Res.*, 2021, **18**, 178–186.
13 M. Shaunak, J. C. Blair and J. H. Davies, *Arch. Dis. Child. Educ. Pract.*, 2020, **105**, 347–351.
14 A. Titman, V. Price, D. Hawcutt, C. Chesters, M. Ali, G. Cacace, G. A. Lancaster, M. Peak and J. C. Blair, *Clin. Endocrinol.*, 2020, **93**, 572–578.

15 A. Levine, O. Zagoory-Sharon, R. Feldman, J. G. Lewis and A. Weller, *Physiol. Behav.*, 2007, **90**, 43–53.
16 Y. Zhou, S. Dliso, J. Craske, A. Gill, L. Bracken, K. Landa, P. Arnold, L. Walker, I. Grasim and G. Seddon, *BMC Med.*, 2024, **22**, 553.
17 Y. Zhou, T.-T. Sham, C. Boisdon, B. L. Smith, J. C. Blair, D. B. Hawcutt and S. Maher, *Analyst*, 2023, **148**, 5366–5379.
18 F. Rossi, T. Trakoolwilaiwan, V. Gigli, C. Tortolini, A. Lenzi, A. M. Isidori, N. T. K. Thanh and R. Antiochia, *Nanoscale*, 2024, **16**, 18134–18164.
19 K. Wang, W. Qin, Y. Hou, K. Xiao and W. Yan, *Nano Biomed. Eng.*, 2016, **8**, 172–183.
20 H.-K. Oh, K. Kim, J. Park, H. Im, S. Maher and M.-G. Kim, *Biosens. Bioelectron.*, 2022, **205**, 114094.
21 H.-K. Oh, J. Park, W. J. Sonstein, S. Maher and M.-G. Kim, *Neurosurgery*, 2024, **95**, 305–312.
22 T. Trakoolwilaiwan, Y. Takeuchi, T. S. Leung, M. Sebek, L. Storozhuk, L. Nguyen, L. D. Tung and N. T. K. Thanh, *Nanoscale*, 2023, **15**, 12915–12925.
23 S. Maher, F. P. Jjunju and S. Taylor, *Rev. Mod. Phys.*, 2015, **87**, 113–135.
24 M. Díaz-González and A. de la Escosura-Muñiz, *Anal. Bioanal. Chem.*, 2021, **413**, 4111–4117.
25 H.-K. Oh, J.-W. Kim, J.-M. Kim and M.-G. Kim, *Analyst*, 2018, **143**, 3883–3889.
26 H.-K. Oh, K. Kim, J. Park, H. Jang and M.-G. Kim, *Sci. Rep.*, 2021, **11**, 22580.
27 J. Langer, D. Jimenez de Aberasturi, J. Aizpurua, R. A. Alvarez-Puebla, B. Auguié, J. J. Baumberg, G. C. Bazan, S. E. Bell, A. Boisen and A. G. Brolo, *ACS Nano*, 2019, **14**, 28–117.
28 V. Tran, B. Walkenfort, M. König, M. Salehi and S. Schlücker, *Angew. Chem., Int. Ed.*, 2019, **58**, 442–446.
29 X. Fu, Z. Cheng, J. Yu, P. Choo, L. Chen and J. Choo, *Biosens. Bioelectron.*, 2016, **78**, 530–537.
30 D. Li, Y. Zhang, R. Li, J. Guo, C. Wang and C. Tang, *Small*, 2015, **11**, 2200–2208.
31 W. J. Cho, Y. Kim and J. K. Kim, *ACS Nano*, 2012, **6**, 249–255.
32 B. Akbali, M. Yagmurcukardes, F. Peeters, H.-Y. Lin, T.-Y. Lin, W.-H. Chen, S. Maher, T.-Y. Chen and C.-H. Huang, *J. Phys. Chem. C*, 2021, **125**, 16289–16295.
33 L. Lin, X. Tian, S. Hong, P. Dai, Q. You, R. Wang, L. Feng, C. Xie, Z. Q. Tian and X. Chen, *Angew. Chem., Int. Ed*, 2013, **52**, 7266–7271.
34 H. K. Lee, Y. H. Lee, C. S. L. Koh, G. C. Phan-Quang, X. Han, C. L. Lay, H. Y. F. Sim, Y.-C. Kao, Q. An and X. Y. Ling, *Chem. Soc. Rev.*, 2019, **48**, 731–756.
35 H. Ko, S. Chang and V. V. Tsukruk, *ACS Nano*, 2009, **3**, 181–188.
36 T. S. Alomar, N. AlMasoud, Y. Xu, C. Lima, B. Akbali, S. Maher and R. Goodacre, *Sensors*, 2022, **22**, 7832.
37 P. K. Jain, X. Huang, I. H. El-Sayed and M. A. El-Sayed, *Acc. Chem. Res.*, 2008, **41**, 1578–1586.
38 T. A. Rocha-Santos, *TrAC, Trends Anal. Chem.*, 2014, **62**, 28–36.
39 E. Y. Ariffin, Y. H. Lee, D. Futra, L. L. Tan, N. H. A. Karim, N. N. N. Ibrahim and A. Ahmad, *Anal. Bioanal. Chem.*, 2018, **410**, 2363–2375.
40 X. Wang, N. Choi, Z. Cheng, J. Ko, L. Chen and J. Choo, *Anal. Chem.*, 2017, **89**, 1163–1169.
41 R. Wang, K. Kim, N. Choi, X. Wang, J. Lee, J. H. Jeon, G.-e. Rhie and J. Choo, *Sens. Actuators, B*, 2018, **270**, 72–79.
42 J. Hwang, S. Lee and J. Choo, *Nanoscale*, 2016, **8**, 11418–11425.
43 W. Maneeprakorn, S. Bamrungsap, C. Apiwat and N. Wiriyachaiporn, *RSC Adv.*, 2016, **6**, 112079–112085.
44 L. Blanco-Covián, V. Montes-García, A. Girard, M. T. Fernández-Abedul, J. Pérez-Juste, I. Pastoriza-Santos, K. Faulds, D. Graham and M. C. Blanco-Lopez, *Nanoscale*, 2017, **9**, 2051–2058.
45 Y. Xie, H. Chang, K. Zhao, J. Li, H. Yang, L. Mei, S. Xu and A. Deng, *Anal. Methods*, 2015, **7**, 513–520.
46 X. Gao, P. Zheng, S. Kasani, S. Wu, F. Yang, S. Lewis, S. Nayeem, E. B. Engler-Chiurazzi, J. G. Wigginton and J. W. Simpkins, *Anal. Chem.*, 2017, **89**, 10104–10110.
47 N. R. Stambach, S. A. Carr, C. R. Cox and K. J. Voorhees, *Viruses*, 2015, **7**, 6631–6641.
48 J. A. Ray, E. Kish-Trier and L. M. Johnson, in *Clinical Applications of Mass Spectrometry in Biomolecular Analysis: Methods and Protocols*, Springer, 2022, pp. 119–128.
49 S. Sloan-Dennison, E. O'Connor, J. W. Dear, D. Graham and K. Faulds, *Anal. Bioanal. Chem.*, 2022, **414**, 4541–4549.
50 W. A. Hassanain, J. Spoors, C. L. Johnson, K. Faulds, N. Keegan and D. Graham, *Analyst*, 2021, **146**, 4495–4505.
51 W. B. Anderson, P. P. Gqamana and Y. V. Zhang, in *Clinical Applications of Mass Spectrometry in Biomolecular Analysis: Methods and Protocols*, ed. U. Garg, Springer US, New York, NY, 2022, DOI: **10.1007/978-1-0716-2565-1_10**, pp. 105–117.
52 B. Khlebtsov and N. Khlebtsov, *Nanomaterials*, 2020, **10**, 2228.
53 E. Gniazdowska, E. Gilant and K. Buś-Kwaśnik, *Prospects Pharm. Sci.*, 2023, **21**, 57–63.
54 A. Roychoudhury, S. Basu and S. K. Jha, *Biosens. Bioelectron.*, 2016, **84**, 72–81.
55 R. Goel, S. Chakraborty, V. Awasthi, V. Bhardwaj and S. K. Dubey, *Sens. Actuators, A*, 2024, 115555.